Article:
Zhang, Z and Gleeson, HF (2019) Understanding liquid crystal order parameters deduced from different vibrations in polarised Raman spectroscopy. Liquid Crystals, 46 (2). pp. 219-233. ISSN: 0267-8292

https://doi.org/10.1080/02678292.2018.1485980

Published in Liquid Crystals 21 Jun 2018 DOI: 10.1080/02678292.2018.1485980

Understanding liquid crystal order parameters deduced from different vibrations in polarized Raman spectroscopy

Zhaopeng Zhang and Helen F. Gleeson

School of Physics and Astronomy, University of Leeds, Leeds, UK

Zhaopeng Zhang, School of Physics and Astronomy, The University of Leeds, Leeds LS2 9JT, UK, phyzz@leeds.ac.uk

Helen F. Gleeson, School of Physics and Astronomy, The University of Leeds, Leeds LS2 9JT, UK, H.F.Gleeson@leeds.ac.uk

Understanding liquid crystal order parameters deduced from different vibrations in polarized Raman spectroscopy

Polarized Raman Spectroscopy (PRS) has been used to measure order parameters in liquid crystalline materials for decades. However, it is well-known that different values of the order parameters are deduced for the same material when different vibrational modes are used in the analysis. This is an undesirable discrepancy that has somewhat hindered the use of the technique. Here we use two Raman active bands namely the phenyl (1606cm^{-1}) and cyano (2220cm^{-1}) stretching modes in the nematic phase of 5CB (4-cyano-4'-pentylbiphenyl) as the example to explore the origin of such discrepancy. Two approaches are proposed in the data analysis taking either non-axial or non-cylindrical symmetric vibration into consideration. Together with a systematic discussion based on experimental data, we can conclude that whether or not the vibration satisfies the conditions associated with cylindrical symmetry is the correct physical explanation for the discrepancy in the order parameters.

Keywords: nematic, Polarized Raman Spectroscopy, order parameter, molecular biaxiality

Dataset: https://doi.org/10.5518/354

Introduction

The dynamic order exhibited by the molecules in a liquid crystal phase is a fundamental property of the liquid crystalline state, and it is the combination of order and fluidity that makes liquid crystals important technological materials. The order is described quantitatively through the order parameter, which is the statistical average obtained by considering the orientational distribution function (ODF); the ODF describes the probability of a liquid crystal molecule adopting a specific orientation. For nematic liquid crystals, the ODF is described in terms of the generalised Legendre polynomials P_{Lmn} and order parameters $\langle P_{Lmn} \rangle$ where the indices L, m and n take integer values. There are many approaches to measuring the order parameter in liquid crystals including electron spin resonance

spectroscopy [1, 2], x-ray[3, 4, 5, 6, 7, 8], optical techniques[9], neutron scattering[10, 11], and analysis of infrared spectra[12, 13, 14] . However, polarized Raman spectroscopy (PRS) is an important optical technique since it can be used to obtain not only the second order term $\langle P_{200} \rangle$, but also the next higher order term with $L = 4$, a parameter that can be obtained by very few other experimental methods[3, 15, 16, 17, 18, 19, 20, 21, 22]. Further, Raman spectroscopy requires no special sample preparation and is a readily accessible laboratory-based technique, further advantages over the other possible approaches to determining $\langle P_{400} \rangle$.

Jen *et al*. initially proposed a method of measuring the order parameter in nematic liquid crystals from Raman spectra using the parallel and perpendicular depolarisation ratio in two experimental arrangements (analyser parallel or perpendicular to the liquid crystal director) in a homogenously aligned sample[16, 17]. The method was shown to work rather well in deducing $\langle P_{200} \rangle$, but sometimes gave negative values for $\langle P_{400} \rangle$, which is far from the predictions made by Maier-Saupe theory[23] or Humphries-James-Luckhurst theory[24]. It was later shown that analysis of the whole range of the depolarisation ratio (intensity ratio between two experiment arrangements where polarizer and analyser are parallel or perpendicular to each other) as a function of rotation angle gives physically realistic values of $\langle P_{400} \rangle$[18, 19, 21, 22]. Further, it was only when the dependence of the differential polarisability ratio, r, on external parameters such as temperature was included in the analysis that values of $\langle P_{200} \rangle$ and $\langle P_{400} \rangle$ in good agreement with theoretical predictions were determined across the nematic range[3, 21]. Consequently it is now accepted that PRS is a robust and reliable technique that can be used to obtain both $\langle P_{200} \rangle$ and $\langle P_{400} \rangle$ in liquid crystals.

Despite the refinements in the experimental approach and data analysis described above, a significant complication remains in the use of PRS to deduce order parameters. It is well known that

the order parameters deduced from different Raman active vibrational bonds are found to be different within the same sample[25]. Indeed, almost all of the liquid crystal order parameter measurements reported in the literature make use of the phenyl stretching mode at 1606 cm^{-1} which clearly satisfies some of the important assumptions that are made in the analysis of the Raman spectra[26]. However, in Ref.25, Miyano pointed out that the shape of a liquid crystal molecule is not uniaxial and that may lead to a non-uniaxial distribution. Further, he mentioned that the cyano stretching mode may potentially have non-cylindrical symmetry, which conflicts with the original assumptions used in Raman analysis which are generally based on Jen's method, necessarily providing limited view of the problem.

We have reviewed all of the assumptions made in the previous approaches [18, 21]. We agree that both the vibrational direction with respect to the main molecular axis and the Raman vibrational symmetry may vary for different vibrational modes. This has lead us to believe that neglecting these features in previous analyses may have led to the discrepancy between the order parameters obtained from different vibrational modes. Consequently, in this paper, we have modified the analysis method by considering non-axial vibration and non-cylindrical vibration symmetry models in order to test our hypothesis. We demonstrate that by including these two features, exactly the same set of order parameters can be obtained from different vibrational modes. Further, by introducing results from molecular simulations, we conclude that of the two possibilities, whether or not the vibration satisfies the conditions of cylindrical symmetry is the correct physical explanation of the discrepancy in the order parameters.

Discrepancy between order parameters obtained from different vibrational modes

As mentioned above [18, 19, 20, 21], several authors have analysed the full depolarisation ratio

determined from PRS to deduce physically realistic values of $\langle P_{200} \rangle$ and $\langle P_{400} \rangle$. In this section, an example of the analysis is shown based on a well-known nematic liquid crystal material 4-cyano-4'-pentylbiphenyl, also known as 5CB. The molecular structure is shown together with its Raman spectrum in Figure 1.

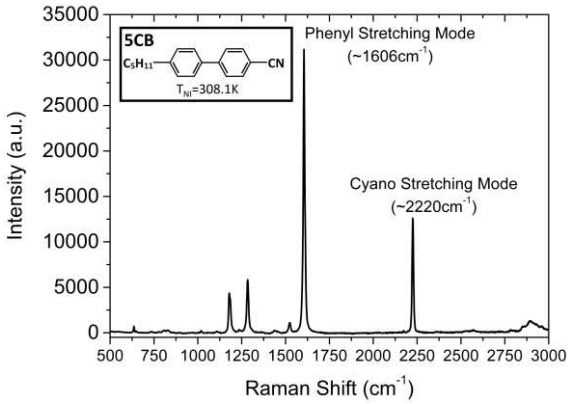

Figure 1. The molecular structure of 4-cyano-4'-pentylbiphenyl (5CB) and its Raman spectrum.

5CB forms a nematic liquid crystal phase at room temperature with the clearing point from nematic phase to isotropic phase, T_{NI} at 308.1 K. The depolarisation data were collected from a homogeneously aligned sample of 5CB using the PRS technique described in Ref.21. A Renishaw 1000 Raman spectrometer equipped with a 515 cm^{-1} solid-state laser with a maximum output power of 50mW was used in the experiment. An ultra-long working distance Olympus x50 objective lens was fitted in the PRS system to collect the Raman spectra. A Linkam hot stage and temperature controller maintain the sample temperature with a relative accuracy of ±0.1 K. The Raman system can measure frequency shifts up to 3000 cm^{-1}, covering the main Raman peaks (1606 cm^{-1} and 2220 cm^{-1}) that occur in the material under study.

In the experiment, a planar-aligned 5CB sample was placed on the rotating stage of the Raman microscope system. Raman spectra were collected at 5° intervals from 0° to 360° for both the

parallel configuration (polarizer and analyser are parallel) and perpendicular configuration (polarizer is perpendicular to the analyser). The intensity of the Raman peak for each configuration, $I_{\parallel}$ and $I_{\perp}$ was deduced by fitting with a Lorentz function. The ratio of the perpendicular to parallel intensity, i.e. the depolarisation ratio, *R*, is thus deduced as a function of rotation angle θ. Eqs. 1 and 2 [18, 21] describe the parallel and perpendicular intensities as a function of rotation angle θ. Fitting the experimentally determined depolarisation ratio plot using Eqs.1 and 2 allows the order parameters $\langle P_{200} \rangle$ and $\langle P_{400} \rangle$ and differential polarisability ratio *r* to be deduced.

$$I_{\parallel} \propto \frac{1}{5} + \frac{4\mathrm{r}}{15} + \frac{8r^2}{15} + \langle P_{200} \rangle \left[\frac{1}{21} (3 + \mathrm{r} - 4\,\mathrm{r}^2)(1 + 3\ \cos 2\theta) \right] + \langle P_{400} \rangle \left[\frac{1}{280} (1 - \mathrm{r})^2\ (9 + 20\ \cos 2\theta + 35 \cos 4\theta) \right], \quad (1)$$

$$I_{\perp} \propto \frac{1}{15} (1 - r)^2 + \langle P_{200} \rangle \left[\frac{1}{21} (1 - r)^2 \right] + \langle P_{400} \rangle \left[\frac{1}{280} (1 - r)^2 (3 - 35 \cos 4\theta) \right]. \quad (2)$$

In previous work, Southern et.al [18, 21] selected the phenyl stretching mode for analysis and, as already mentioned, this results in the determination of order parameters that are in good agreement both with theory and with other experimental approaches as shown in Figure 2. The theory curve is obtained from Humphries-James-Luckhurst theory[24] which gives an estimate of order parameters in a uniaxial liquid crystal system.

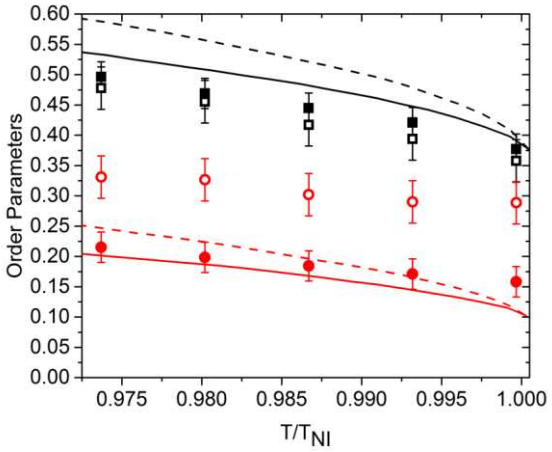

Figure 2. Plot of $\langle P_{200} \rangle$ (squares) and $\langle P_{400} \rangle$ (circles) values versus temperature compared with the Humphries-James-Luckhurst theoretical predictions [24] (dashed line: $\lambda = 0.15;\ \gamma = 2$ and solid line $\lambda = 0.15;\ \gamma = 0$). The order parameters deduced from the phenyl stretching mode at 1606cm^{-1} and the cyano stretching mode at 2220cm^{-1} are defined by the filled and open symbols respectively.

Despite the success of using the phenyl stretching mode in the analysis, it has long been known that the values obtained from other vibration modes may give different values of the order parameters[25]. Indeed, use of the cyano stretching mode, another important Raman active vibration at 2220cm^{-1}, readily show this discrepancy (Figure 2) where the $\langle P_{400} \rangle$ values obtained from the cyano stretching mode are far from both the phenyl stretching mode data and the theoretical predictions. To give a deeper insight, Figure 3 shows a comparison of depolarisation ratio plots obtained from both the phenyl stretching and cyano stretching modes. It is clear that the depolarisation ratio plots are different, leading to the difference in order parameters deduced from the two vibrational modes. We ruled out the possibility that the difference is a consequence of antiparallel ordering of the molecules, which is a well-known effect in 5CB, by equivalent measurements in the liquid crystal mixture E63, designed to remove antiparallel ordering. The depolarisation ratios shown in Figure 3 are similar for both liquid crystal mixtures, indicating that

differences in local environments of the molecules is not an explanation for the discrepancies in order parameter.

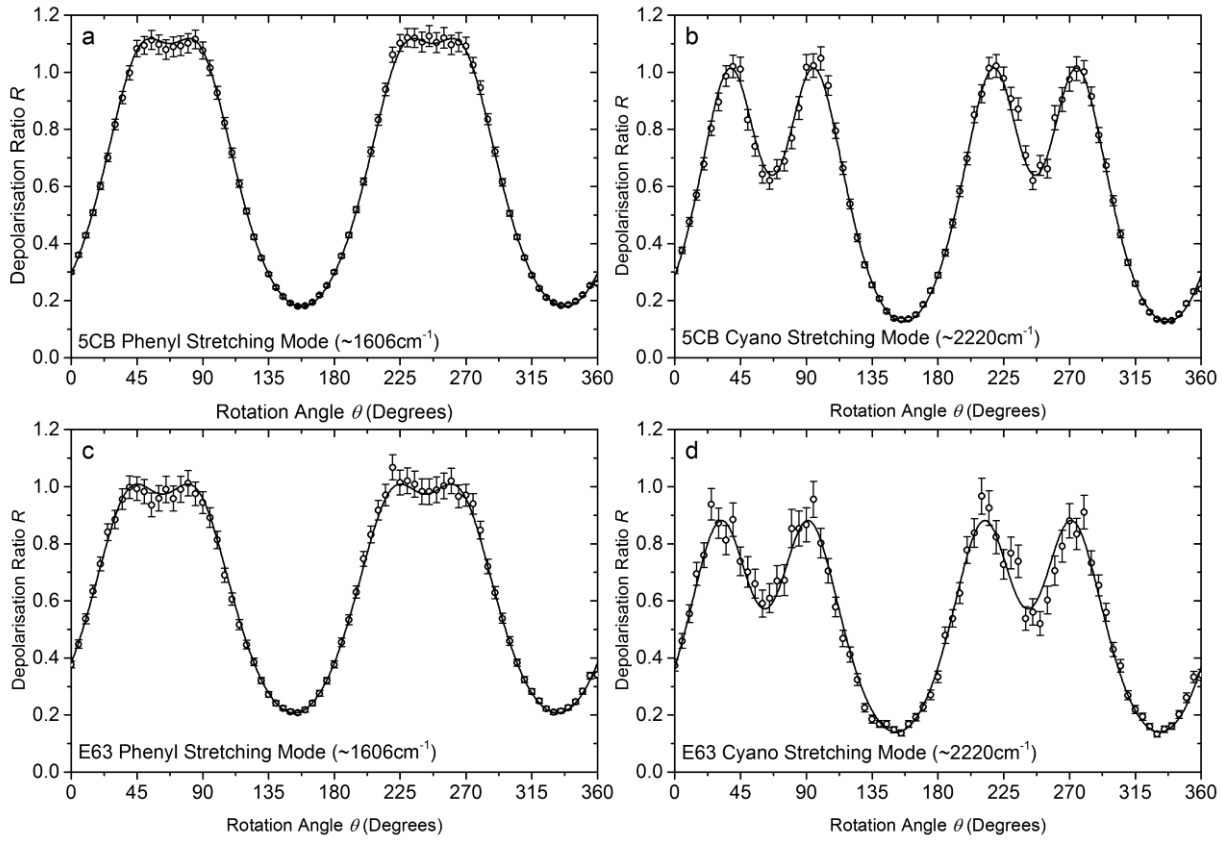

Figure 3. Experimental data and the fits to Eqs. 1 and 2. a) and c) show the depolarisation ratio as a function of rotation angle, deduced for the phenyl stretching mode at 1606 cm^{-1}, while b) and d) are for the cyano stretching mode at 2220 cm^{-1}. a) and b) are collected from the 5CB sample at 304K (0.987 T/T_{NI}). c) and d) are collected from the E63 sample at 354K (0.985T/T_{NI}).

Non-axial model

As mentioned in the previous section, there are clearly discrepancies in applying the usual analysis of the depolarisation ratios to deducing order parameters from vibrations other than the phenyl stretch as the analysis method relies on some key assumptions, in particular, one is that the Raman active

bond vibrational direction aligns with the molecular long axis. To clarify this point, firstly, note that the molecular long axis is normally considered as the direction of the biphenyl rigid core of the liquid crystal molecule as the terminal alkyl chain is flexible and its statistically averaged direction is expected to be in line with the biphenyl core. Secondly, the vibrational direction is normally considered to be the direction of the special axis in which the Raman tensor, normally a 3 by 3 matrix, can be expressed as a diagonal matrix. We maintain this condition that the vibrational direction defines the frame where the Raman tensor is diagonal. However, we also need to consider whether the different vibrational modes, i.e. the cyano stretching mode and phenyl stretching mode, have different vibrational directions.

First of all, we need to consider a more generalized model to analyze the PRS data. As shown in Figure 4, there are four relevant frames, the vibration frame, V, with a component z_V along the vibration direction; the molecular frame M which uses the molecular long axis as its z_M axis; the director frame D in which the component z_D is along director direction; and the laboratory frame L with the $x_L, O", z_L$ plane where the liquid crystal sample rotates in and y_L is the laser incidence direction. The Euler angle between the vibrational frame and molecular frame, the molecular frame and director frame and the director frame and laboratory frame are $(0, \beta_0, 0)$, (α, β, γ) and $(0, \theta, 0)$ respectively. This model is based on three assumptions: the liquid crystal system is a uniaxial system; the liquid crystal molecule can be biaxial or board like as shown in Figure 4; the vibration itself has uniaxial symmetry. Combining all the assumptions, the ODF can be written as given in Eq.3[26, 27]. Here, P_{L0n} are a set of generalised Legendre polynomials with the mean value $\langle P_{L0n} \rangle$ describing the order property. This equation indicates the possibility of one molecule pointing in a direction defined by Euler angles (α, β, γ). Notice that in this equation, there is no α related term. This is because the phase is uniaxial so there is no α dependence on the molecular distribution.

Following a similar approach as discussed in Ref. 20 we can obtain the final expressions for $I_{\parallel}$ and $I_{\perp}$ as shown in Eqs. 4 and 5, which depend on the parameters r, β_0, θ, $\langle P_{200}\rangle$, $\langle P_{202}\rangle$, $\langle P_{400}\rangle$, $\langle P_{402}\rangle$ and $\langle P_{404}\rangle$, where $\langle P_{200}\rangle$ and $\langle P_{400}\rangle$ are uniaxial order parameters. Here, $I_{\parallel}$ and $I_{\perp}$ indicate the intensity obtained with analyser parallel and perpendicular to the laser polarisation direction respectively. Since the vibration is away from the molecular long axis, the molecules can be regarded as board-like, the molecules arrangement may be confined by the structure, so there could be a distribution according to the molecular rotation position, thus the molecular biaxial order parameters. $\langle P_{202}\rangle$, $\langle P_{402}\rangle$ and $\langle P_{404}\rangle$ appear in the equation. It is worth noticing that here we are considering the most generalized situation, where the molecular biaxiality is included. However, we are not ruling out the special situation where all molecular biaxial order parameters equal zero. In this case, although the molecules are board-like, the molecules are still rotationally free, i.e. no molecular biaxiality properties persist.

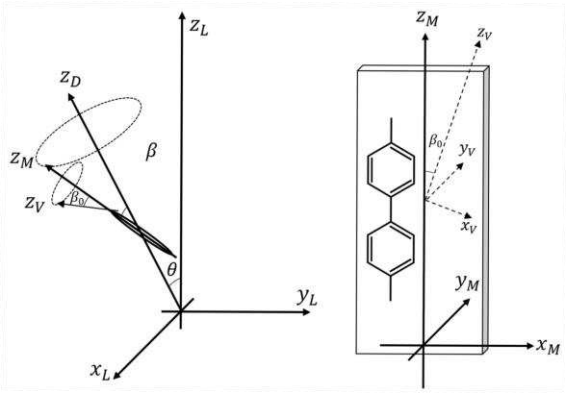

Figure 4. Four frames exist in our analysis: the laboratory frame (x_L, y_L, z_L); the director frame (x_D, y_D, z_D); the molecular frame (x_M, y_M, z_M); and the vibration frame (x_v, y_v, z_v).

$$f(\beta,\gamma)=\left(\frac{1}{8\pi^2}\right)\begin{pmatrix} 1+\frac{5}{2}\langle P_{200}\rangle(3\cos^2\beta-1) \\ +\frac{5}{2}\langle P_{202}\rangle 6(1-\cos^2\beta)\cos(2\gamma) \\ +\frac{9}{8}\langle P_{400}\rangle(35\cos^4\beta-30\cos^2\beta+3) \\ +\frac{9}{8}\langle P_{402}\rangle 60(7\cos^2\beta-1)(1-\cos^2\beta)\cos(2\gamma) \\ +\frac{9}{8}\langle P_{404}\rangle 70(1-\cos^2\beta)^2\cos(4\gamma) \end{pmatrix}. \quad (3)$$

$$I_{\parallel}\propto\frac{1}{5}+\frac{4\mathrm{r}}{15}+\frac{8r^2}{15}+\langle P_{200}\rangle\left[\frac{1}{84}(3+\mathrm{r}-4\,\mathrm{r}^2)(1+3\ \cos 2\beta_0)(1+3\ \cos 2\theta)\right]$$
$$+\langle P_{400}\rangle\left[\frac{1}{17920}(-1+\mathrm{r})^2\ (9+20\ \cos 2\beta_0+35\ \cos 4\beta_0)(9+20\ \cos 2\theta\right.$$
$$\left.+35\cos 4\theta)\right]+\langle P_{202}\rangle\left[\frac{1}{7}\ (3+\mathrm{r}-4\,\mathrm{r}^2)(1+3\ \cos 2\theta)(\sin\beta_0)^2\right]$$
$$+\langle P_{402}\rangle\left[\frac{3}{224}\ \ (-1+\mathrm{r})^2\ (5+7\ \cos 2\beta_0)(9+20\ \cos 2\theta+35\ \cos 4\theta)(\sin\beta_0)^2\right]$$
$$+\langle P_{404}\rangle\left[\frac{1}{32}\ \ (-1+\mathrm{r})^2\ (9+20\ \cos 2\theta+35\ \cos 4\theta)(\sin\beta_0)^4\right], \quad (4)$$

$$I_{\perp}\propto\frac{1}{15}(-1+r)^2+\langle P_{200}\rangle\left[\frac{1}{84}(-1+r)^2(1+3\cos 2\beta_0)\right]$$
$$+\langle P_{400}\rangle\left[-\frac{1}{17920}(-1+r)^2(9+20\cos 2\beta_0+35\cos 4\beta_0)(-3+35\cos 4\theta)\right]$$
$$+\langle P_{202}\rangle\left[\frac{1}{7}(-1+r)^2(\sin\beta_0)^2\right]$$
$$+\langle P_{402}\rangle\left[-\frac{3}{224}(-1+r)^2(5+7\cos 2\beta_0)(-3+35\cos 4\theta)(\sin\beta_0)^2\right]$$
$$+\langle P_{404}\rangle\left[-\frac{1}{32}(-1+r)^2(-3\right.$$
$$\left.+35\cos 4\theta)(\sin\beta_0)^4\right]. \quad (5)$$

If we set $\beta_0 = 0$, all $\sin\beta_0$ terms are zero, thus Eqs. 4 and 5 reduce exactly to Jones' equations[18]. This is exactly as would be expected; if no vibration tilt exists, our board-like molecular model will degenerate to a uniaxial rod-like molecular model. On the other hand, if we set all the order parameters to be zero as will occur in the isotropic phase, the intensities becomes equivalent as expected in isotropic phase [17]. Finally, the depolarisation ratio *R* measured experimentally can be obtained by taking the ratio of Eqs. 4 and 5:

$$R = \frac{I_{\perp}}{I_{\parallel}}. \tag{6}$$

Discussion of the effect on the depolarisation ratio plot

The effect of $\langle P_{200}\rangle$ and $\langle P_{400}\rangle$ on the form of the dependence of depolarisation ratio on angle θ has been discussed previously [18], and the influence of the higher order terms was considered briefly[9], while maintaining the original assumptions. Here we use Eqs. 4 and 5 to evaluate the influence of the parameters $\langle P_{202}\rangle$, $\langle P_{402}\rangle$, $\langle P_{404}\rangle$ and β_0 on the form of the depolarisation ratio while no longer making the fundamental assumptions. Significant insight can be obtained by calculating the depolarisation ratio curves and Figure 5 shows the effect each parameter has on these curves. We first want to discuss the case where no molecular biaxiality is included. In this case, all of the $\langle P_{202}\rangle$, $\langle P_{402}\rangle$ and $\langle P_{404}\rangle$ terms are set to zero in Eqs. 4 and 5 and only vibrational tilt β_0 is introduced. Figure 5(a) shows the effect of β_0. It is clear that β_0 causes a change in the depolarisation ratio plot. However considering β_0 only will not generate the difference in depolarisation ratio that can be seen in Figure 3. In fact, considering β_0 makes the curve fluctuate less, is contrary to the effect on the depolarisation ratio curve seen in Figure 3. This leads us to believe the molecular biaxiality is necessary for the discussion. The effect of each of the molecular biaxial order

parameters can be summarized as follows:

- Increasing $\langle P_{202} \rangle$, Figure 5(b) causes a increase in the depolarisation ratio around the θ=90° and θ=270° positions while other regions scarcely change. This outcome is similar to an increase $\langle P_{200} \rangle$ with the original assumptions.
- Increasing $\langle P_{402} \rangle$, Figure 5(c) reduces in the depolarisation ratio significantly at θ=90° and 270°, slightly at θ=0° and θ=180°. This effect is very reminiscent of the different fluctuate depolarisation data from the phenyl stretching and cyano stretching modes as shown in Figure 3. Combining the similar effect of increasing $\langle P_{200} \rangle$ with the original assumptions, an important consequence is that increasing $\langle P_{402} \rangle$ would allow the value of $\langle P_{400} \rangle$ deduced from the fit to be reduced, i.e. $\langle P_{402} \rangle$ has an important role in modifying the $\langle P_{400} \rangle$ value.
- $\langle P_{404} \rangle$ (Figure 5(d)) does not have a strong effect on the depolarisation ratio plot. Thus $\langle P_{404} \rangle$ is taken to be zero in the following fitting process.

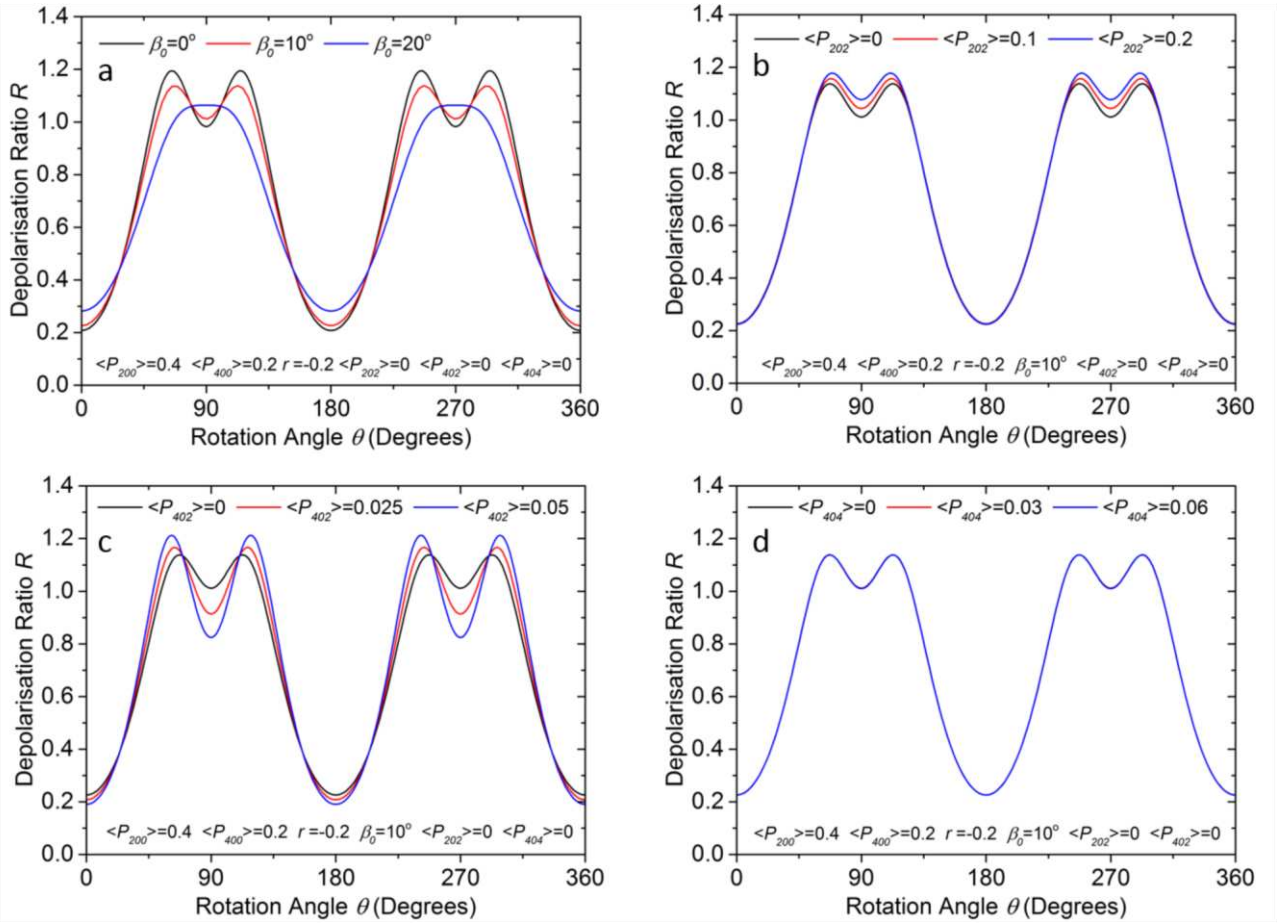

Figure 5. Effect of different order parameters and the vibrational tilt on the form of the dependence of the depolarisation ratio evaluated using Eqs. 4 and 5. In these calculations, $\langle P_{200}\rangle$=0.4; $\langle P_{400}\rangle$=0.2; $r = -0.2$. a) dependence on $\beta_0 = 0°$ (black), 10° (red) and 20° (blue) while all molecular biaxial order parameters are set to zero. b) dependence on $\beta_0 = 10°$, $\langle P_{202}\rangle = 0$ (black), 0.1 (red) and 0.2 (blue); c) dependence on $\beta_0 = 10°$, $\langle P_{402}\rangle = 0$ (black), 0.025 (red) and 0.050 (blue); and d) dependence on $\beta_0 = 10°$, $\langle P_{404}\rangle = 0$ (black), 0.03 (red) and 0.06 (blue).

Discussion of the effect of changing each parameter on the order parameter fits

It is important to have a systematic check of the influence of each parameter in the fitting process and the resultant order parameters. However, the existence of seven fitting parameters makes robust fitting impossible, so in this discussion, we systematically vary the molecular biaxial order parameters and consider how the vibrational tilt β_0 and molecular biaxial order parameters influence

the fitting result for uniaxial order parameters. In this process, $\langle P_{200} \rangle$ and $\langle P_{400} \rangle$ are obtained from fitting the experimental data using Eqs. 4 and 5 with different given values of vibrational tilt β_0 and the constant molecular biaxial order parameter values indicated in Figure 6 (5CB data at 300K).

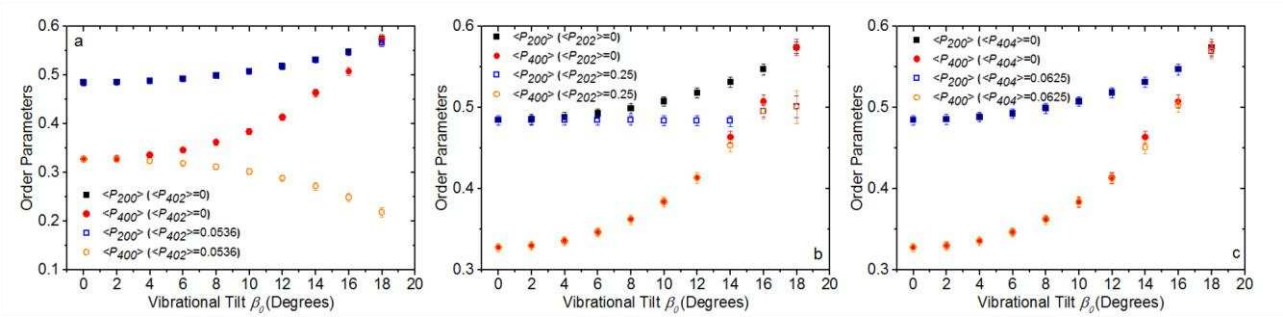

Figure 6. Effect of the vibrational tilt on the uniaxial order parameters obtained from fitting 5CB data at 300K. In these plots, $\langle P_{200} \rangle$ and $\langle P_{400} \rangle$ are represented by squares and circles respectively. (a) $\langle P_{402} \rangle = 0$ (filled symbols) and 0.0536 (empty symbols), $\langle P_{202} \rangle$ and $\langle P_{404} \rangle$ are set to zero; (b) $\langle P_{202} \rangle$ =0 (filled symbols) and 0.25 (empty symbols), $\langle P_{402} \rangle$ and $\langle P_{404} \rangle$ are set to zero; (c) $\langle P_{404} \rangle = 0$ (filled symbols) and 0.0625 (empty symbols), $\langle P_{202} \rangle$ and $\langle P_{402} \rangle$ are set to zero.

From Figure 6, it is shown again that the considering vibrational tilt β_0 alone will not reduce but rather increase the fitting value of $\langle P_{400} \rangle$ as we concluded in last section. According to Figure 6(a), it is clear that $\langle P_{402} \rangle$ has an effect on the fit for $\langle P_{400} \rangle$. $\langle P_{402} \rangle$ can efficiently reduce $\langle P_{400} \rangle$ without changing $\langle P_{200} \rangle$ when the vibrational tilt β_0 becomes larger than $\sim 10^{\circ}$, but does not have a strong influence when the vibrational tilt is small $\beta_0 \leq 5^{\circ}$. Combining this observation with the fact that $\langle P_{402} \rangle$ can lead the depolarisation ratio plot change as same way as was observed experimentally for the cyano stretching mode, leads us to conclude that omitting both molecular biaxial order parameters and the vibrational tilt in the calculation of the order parameters is likely to have caused the discrepancies shown in Figure 3. Further, it suggests that for the phenyl stretching mode, the vibrational tilt β_0 is either zero or small, and neglecting it has very little influence on $\langle P_{400} \rangle$. Conversely, for the cyano stretching mode, the vibrational tilt β_0 is large enough to causes the

divergence of $\langle P_{400} \rangle$ from theory. Figure 6(b) shows the effect of $\langle P_{202} \rangle$ when different vibrational tilt values are introduced. Now $\langle P_{400} \rangle$ is unaffected by the different values of $\langle P_{202} \rangle$, though it increases as the vibrational tilt increases. On the other hand, $\langle P_{200} \rangle$ does depend on both $\langle P_{202} \rangle$ and the vibrational tilt $\beta_0 > 10°$. With the help of both $\langle P_{202} \rangle$ and the vibrational tilt β_0, $\langle P_{200} \rangle$ can stay almost constant, as can be seen in Figure 6(b), which is exactly what we expect physically. Finally it can be seen from Figure 6(c) that $\langle P_{404} \rangle$ does not have strong effect on $\langle P_{200} \rangle$ and $\langle P_{400} \rangle$ as expected.

Discussion of the modified fitting process.

Here we will give some results on a new fitting method based on new versions Eqs. 4 and 5. First we note that some of the parameters are limited by definition, and in particular, the conditions below must be satisfied[27].

$$0 \leq \langle P_{200} \rangle \leq 1;\ 0 \leq \langle P_{400} \rangle \leq 1; \tag{7}$$

$$0 \leq \langle P_{202} \rangle \leq 0.25;\ 0 \leq \langle P_{402} \rangle \leq 0.0536;\ \ 0 \leq \langle P_{404} \rangle \leq 0.0625. \tag{8}$$

Even setting $\langle P_{404} \rangle$ to zero as suggested by the previous section, there are still too many parameters to allow robust fitting. However, it is still possible to use these calculations to explore why the order parameters obtained from different vibration bonds are different.

Data relating to the 5CB cyano stretching mode and phenyl stretching mode are used to illustrate our approach. $\langle P_{200} \rangle$ and $\langle P_{400} \rangle$ are first obtained by using Jones' method[18]. Then $\langle P_{200} \rangle$ is assumed remain unchanged to reduce the number of fitting parameters, justified as $\langle P_{200} \rangle$ values obtained from both the modes are not very different (see Figure 2). The data are then fitted using Eqs. 4 and 5 with $\langle P_{400} \rangle$ initially set to the same value as obtained from the phenyl stretching mode;

the initial values for β_0, $\langle P_{202} \rangle$ and $\langle P_{402} \rangle$ are 10°, 0.25 and 0.0536 respectively. It must be pointed out that as changing $\langle P_{402} \rangle$ can also efficiently modify the $\langle P_{400} \rangle$ value, while maintaining the depolarisation ratio curve, thus there is considerable interdependency between these two parameters, which leads to a large fitting uncertainty for both parameters.

The resulting order parameters are shown in Figure 7and Figure 8 together with the results obtained for $\langle P_{200} \rangle$ and $\langle P_{400} \rangle$ using Jones' method and the fitting results for the phenyl stretching mode. Figure 7 shows that the order parameter values obtained from the cyano stretching mode using Jones' method are far from the theoretical prediction according to Maier-Saupe theory [23] as well as HJL theory [24] while the order parameter values obtained from the different vibrational modes using the new approach are closer to theory predication.

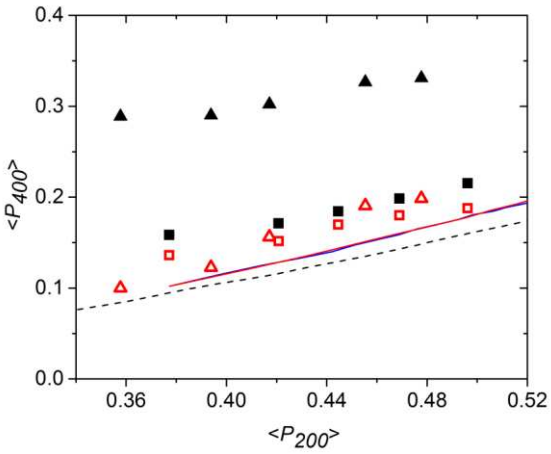

Figure 7. Fitting result comparison. The black line is the theoretical curve from Maier-Saupe mean-field theory while the red and blue solid line from HJL theory ($\lambda = 0.15;\ \gamma = 0$ and $\lambda = 0.15;\ \gamma = 2$ respectively). The filled symbols are the fitting results from Jones' method and the empty symbols are from the new fitting method. The square and the triangle data indicate phenyl and cyano stretching modes respectively.

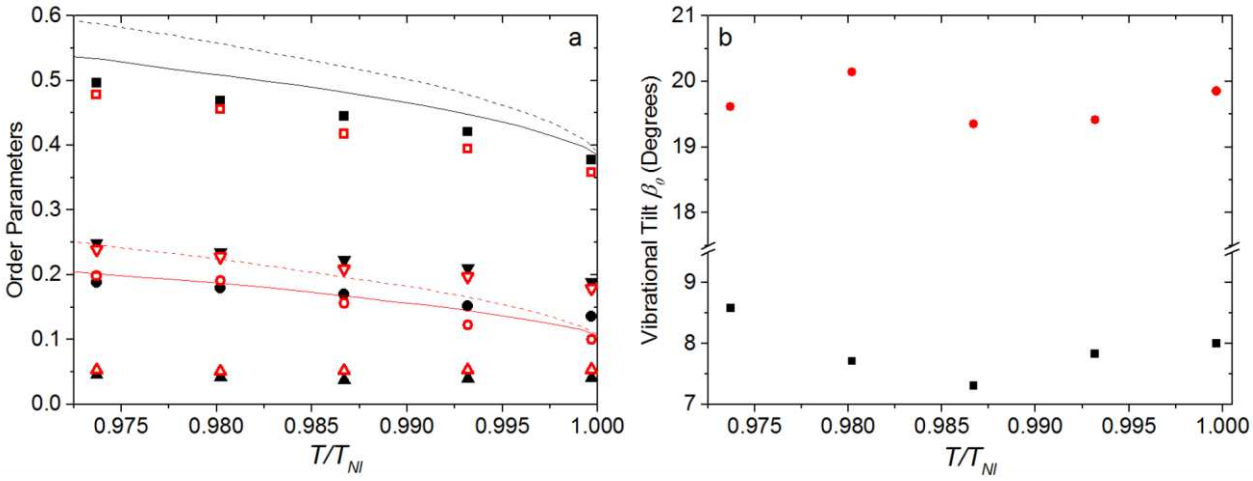

Figure 8. a).The variation of the order parameter as a function of T/T_{NI} where T_{NI} is the nematic to isotropic phase transition temperature. The solid symbols are deduced from fitting to the data for the phenyl-stretching mode, while the open symbols relate to the cyano stretching mode. The data with same label shape represent values for $\langle P_{200} \rangle$ (squares), $\langle P_{202} \rangle$ (inverted triangles), $\langle P_{400} \rangle$ (circles) and $\langle P_{402} \rangle$ (traingles) respectively from top to bottom. The dashed line and solid line are theoretical predictions based on HJL theory for $\langle P_{200} \rangle$ and $\langle P_{400} \rangle$ with $\lambda = 0.15;\ \gamma = 2$ and $\lambda = 0.15;\ \gamma = 0$ respectively. b). Fitting result for vibrational tilt β_0 for cyano stretching mode (circle) and phenyl stretching mode (square).

In Figure 8(a), the deduced values of $\langle P_{200} \rangle, \langle P_{202} \rangle, \langle P_{400} \rangle$ and $\langle P_{402} \rangle$ are shown as a function of temperature. It can be seen from the figure that the order parameters deduced from the phenyl and cyano stretching modes are now in good agreement. It is interesting to note that $\langle P_{202} \rangle$ shows a similar, decreasing tendency when the temperature is increased as occurs for $\langle P_{200} \rangle$ and $\langle P_{400} \rangle$. However, such behaviour is not clear in the data for $\langle P_{402} \rangle$. Taking all of the issues into account, we suggest that there is a strong evidence to indicate that the introduction of the vibrational tilt β_0 reduces the discrepancy previously observed between the order parameter values deduced from different vibration bonds. More importantly, it is possible to obtain similar values of $\langle P_{200} \rangle$ and $\langle P_{400} \rangle$ from the different vibrational bonds if we include vibrational tilt. In addition, as shown in Figure 8(b) we find that the vibrational tilt angle parameter obtained is almost constant

with respect to the temperature change, with β_0=19.7±0.3° for cyano stretching mode and 7.9±0.4° for phenyl stretching mode.

So far, we have not discussed the uncertainties that are inherent in the fitting process in this section and it is important to recognize that there are uncertainties on the values of order parameter deduced from the fits which would normally be included as error bars on the order parameters in Figure 7 and Figure 8. Due to the complexity of the equations, the uncertainties from fitting are hard to systematically analyse. So the fitting results shown above is a supplementary illustration to show that exactly same set of order parameters are possibly to obtain by the new approach.

Simulation

It can be seen from the discussion above that the inclusion of a vibrational tilt both modifies the equations that must be used in the analysis of the depolarisation ratio deduced from PRS, and consequently allows the $\langle P_{200} \rangle$ and $\langle P_{400} \rangle$ order parameters deduced from different vibrational bonds to be self-consistent. However, it is important to give a physical justification to including such a vibrational tilt, as it is unreasonable to simply include additional fitting parameters in the analysis. The vibrational tilt, β_0 can be investigated using molecular simulation software. The program we used is Material Studio and the simulation is based on the DMol3 model which is an ab-initio method. The simulation results give information on all vibrational modes that are present in the chosen molecule, together with their vibrational frequency. The phenyl and cyano stretching modes are of particular relevance to this study. As mentioned, the molecular long axis is defined to be the phenyl stretching direction, and assumes that the contributions from the alky chain average to same axis, along the rigid molecular core. Figure 9 shows the results of the simulation of the phenyl and cyano stretching vibrations. Both vibrations occur in the same direction, i.e. both are along the

molecular long axis. However, this result would seem to imply that vibrational tilt β_0, defined as the tilt angle between the vibrational direction and molecular long axis, cannot explain the discrepancy between the order parameter data deduced from the two different vibrational modes, which are each in the same direction. It is worth noticing that in our discussion, we considered that the molecular long axis follows the biphenyl structure. Also our discussion is based on the statement that the vibration direction aligns with the 'special axis bond' in the diagonal form of the Raman tensor. For the former situation, even if the molecular long axis and the direction biphenyl structure are different, given the fact that the cyano stretching and phenyl stretching modes follow same direction, the vibrational tilt should be identical for these two vibrational modes. This implies, perhaps unsurprisingly, that including the parameter β_0 does not give us a physically realistic explanation for the order parameter discrepancies even though it could provide a mathematical explanation.

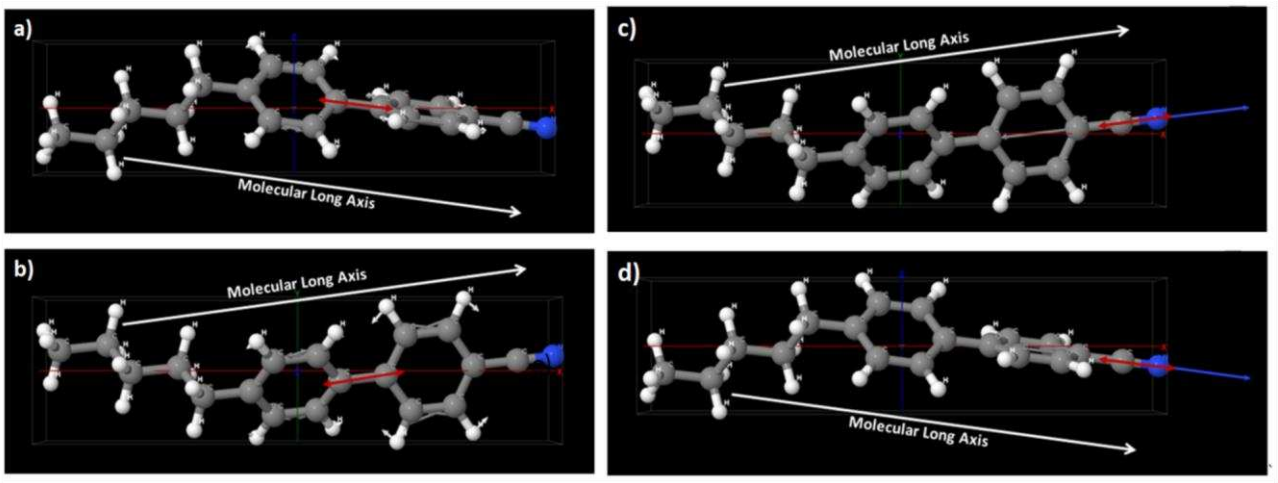

Figure 9. Vibrational directions for: a) and b), the phenyl stretching mode; c) and d), the cyano stretching mode determined from the ab-initio simulations.

Non-cylindrically vibration symmetry model

As shown in previous discussion, although the above analysis offers an interesting possible insight into the discrepancy between order parameters deduced from different Raman-active modes, it is not

likely that it constitutes a solution to the problem at the moment. This is because in the analysis above, the fitting value of $\langle P_{402} \rangle$ always reaches its upper bound of what the definition allows, which is unphysical. We also compare the fitting value to the LZNS theory[28] which gives theoretical predications of molecular biaxial order parameters. As shown in Figure 10, the fitting values we obtained are indeed much higher than theory predicts. Additionally, the fitting value of the vibrational tilts (β_0=19.7±0.3° for cyano stretching mode and 7.9±0.4° for phenyl stretching mode) are much larger than suggested by the modeling (and intuitively expected). Consequently it is important to consider other potential explanations for the order parameter discrepancy. Since introducing molecular biaxiality shows a significant effect, we consider other ways in which this might contribute to the physical system. In this section, we will consider the effect of removing the assumption of cylindrical symmetry of the Raman tensor. For clarity, we will ignore the vibrational tilt for all of the following discussion.

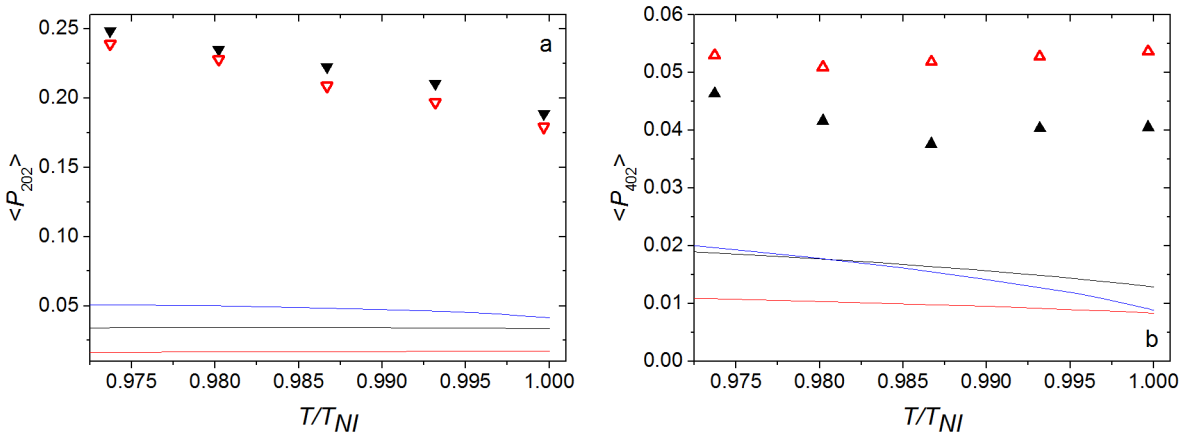

Figure 10. The variation of a). $\langle P_{202} \rangle$ and b). $\langle P_{402} \rangle$ as a function of T/T_{NI} where T_{NI} is the nematic to isotropic phase transition temperature. The solid symbols are deduced from fitting to the data for the phenyl-stretching mode, while the open symbols relate to the cyano stretching mode. The solid lines are theoretical predictions of the biaxial order parameters based on LZNS theory with $\lambda = 0.1$ (red), $\lambda = 0.2$ (blue) and $\lambda = 0.3$ (black).

It is commonly assumed in Raman analysis that the vibration is cylindrically symmetric and the resulting Raman tensor for such vibration in the diagonal form given by Eq.9,

$$\alpha'_S = \begin{pmatrix} \alpha'_{S_{xx}} & 0 & 0 \\ 0 & \alpha'_{S_{yy}} & 0 \\ 0 & 0 & \alpha'_{S_{zz}} \end{pmatrix} = \begin{pmatrix} r\alpha'_{S_{zz}} & 0 & 0 \\ 0 & r\alpha'_{S_{zz}} & 0 \\ 0 & 0 & \alpha'_{S_{zz}} \end{pmatrix} = \begin{pmatrix} r & 0 & 0 \\ 0 & r & 0 \\ 0 & 0 & 1 \end{pmatrix} \alpha'_{S_{zz}}. \quad (9)$$

It is clear that in order to support this assumption, the condition $\alpha'_{S_{xx}} = \alpha'_{S_{yy}}$ must be satisfied. However, it is worthwhile questioning whether this condition is valid for all vibrational modes. In fact, in Jen's paper, he mentioned that the non-cylindrical vibrational symmetry commonly exist [17] and Miyano state that both cyano stretching and biphenyl stretching mode are biaxial in his paper [25]. Thus here we have removed the assumption of cylindrical symmetry and use a generalized non-cylindrical vibrational symmetry model. In such model, $\alpha'_{S_{xx}} \neq \alpha'_{S_{yy}}$ and the Raman tensor can be expressed as,

$$\alpha'_S = \begin{pmatrix} \alpha'_{S_{xx}} & 0 & 0 \\ 0 & \alpha'_{S_{yy}} & 0 \\ 0 & 0 & \alpha'_{S_{zz}} \end{pmatrix} = \begin{pmatrix} a\alpha'_{S_{zz}} & 0 & 0 \\ 0 & b\alpha'_{S_{zz}} & 0 \\ 0 & 0 & \alpha'_{S_{zz}} \end{pmatrix} = \begin{pmatrix} a & 0 & 0 \\ 0 & b & 0 \\ 0 & 0 & 1 \end{pmatrix} \alpha'_{S_{zz}}, \quad (10)$$

The derivation for intensity expression is simpler as no vibrational tilt introduced. After some manipulations, the expression for scattered Raman intensity can be write as Eqs.11 and 12.

$$I_{\parallel} \propto \frac{1}{15}\left(3 + 3a^2 + 2b + 3b^2 + 2a(1+b)\right)$$

$$-\frac{1}{42}\langle P_{200}\rangle(-6 + 3a^2 - b + 3b^2 + a(-1+2b))(1 + 3\cos 2\theta)$$

$$+\frac{1}{2240}\langle P_{400}\rangle(8+3a^2+2a(-4+b)-8b+3b^2)(9+20\,cos\,2\theta+35\,cos\,4\theta)$$

$$+\frac{1}{7}\langle P_{202}\rangle(a-b)(1+3a+3b)(1+3\,cos\,2\theta)$$

$$-\frac{3}{112}\langle P_{402}\rangle(a-b)(-2+a+b)(9+20\,cos\,2\theta+35\,cos\,4\theta)$$

$$+\frac{1}{32}\langle P_{404}\rangle(a-b)^2(9+20\,cos\,2\theta+35\,cos\,4\theta) \tag{11}$$

$$\mathrm{I}_{\perp}\propto\frac{1}{15}(1+a^2-b+a^2-a(1+b))$$

$$-\frac{1}{42}\langle P_{200}\rangle(-2+a^2+a(2-4b)+2b+b^2)$$

$$-\frac{1}{2240}\langle P_{400}\rangle(8+3a^2+2a(-4+b)-8b+3b^2)(-3+35\,cos\,4\theta)$$

$$+\frac{1}{7}\langle P_{202}\rangle(a-b)(-2+a+b)$$

$$+\frac{3}{112}\langle P_{402}\rangle((a-b)(-2+a+b)(-3+35\,cos\,4\theta)$$

$$-\frac{1}{32}\langle P_{404}\rangle(a-b)^2(-3+35\,cos\,4\theta) \tag{12}$$

As Eqs. 11 and 12 show, the molecular biaxial order parameters again appear in the intensity expression as the vibration is no longer cylindrically symmetric which means they may no longer rotational independent. Also, interestingly, all biaxial terms appear alongside the term $(a-b)$ and so they only affect the intensity expression when $a \neq b$.

Discussion of the effect on the depolarisation ratio plot

In this section, the effect of each molecular biaxial order parameter and polarisability ratios will be discussed. As both differential polarisability ratios a and b will affect the depolarisation ratio plot and need to be considered at the same time, we use contour plots for the discussion and we only show two depolarisation ratio values at the rotational angles $\theta = 0°$ and $\theta = 90°$. In all the following discussion, $\langle P_{200} \rangle$ and $\langle P_{400} \rangle$ are set to be 0.5 and 0.2 respectively which is a reasonable value based on theory. As in previous section, we want to discuss the simplest situation first which ignores all molecular biaxiality but check the effect on the two differential polarisability ratios. It is worth noticing that this is exactly the case discussed by Jen in his paper [17]. Figure 11 indicates the contour plots of the calculated depolarisation ratio value according to Eqs. 11 and 12 at $\theta = 0°$ and $\theta = 90°$ with all molecular biaxial order parameters set zero. According to these plots, the depolarisation ratio, R, values are symmetric to the line $a = b$. This indicates the effect of a and b are identical on the depolarisation ratio. The R value at $\theta = 0°$ always increases if either a or b decreases according to Figure 11(a). The R value change is more complex at $\theta = 90°$ such that the R reaches a maximum at around $a = b = -0.2$ and then decreases with any change of a and b, as Figure 11(b) shows.

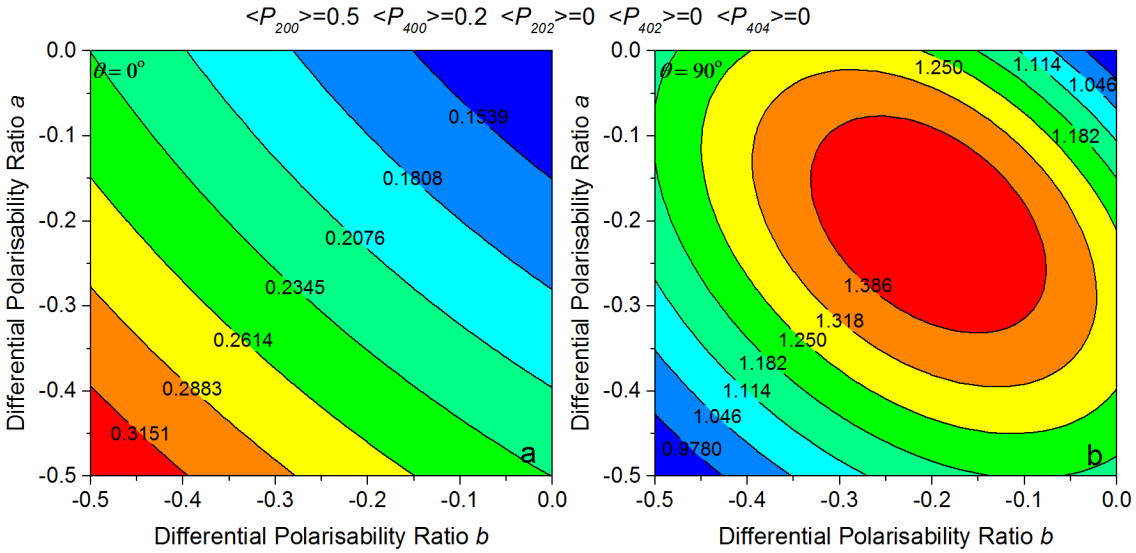

Figure 11. The contour plot of the depolarisation ratio R at: a) $\theta = 0°$ and b) $\theta = 90°$ with $\langle P_{200} \rangle = 0.5$, $\langle P_{400} \rangle = 0.2$, $\langle P_{202} \rangle = 0$, $\langle P_{402} \rangle = 0$ and $\langle P_{404} \rangle = 0$. The x axis and y axes are the differential polarisability ratios b and a respectively.

Now we move to the effect of the molecular biaxial order parameters. Figure 12 indicates the contour plots when $\langle P_{202} \rangle = 0.25$ while all other molecular biaxial order parameters were set to zero. The contour plots are no longer symmetric about the line a=b due to the $(a - b)$ term and existance of $\langle P_{202} \rangle$ though the values on the line where $a = b$ are unchanged. Comparing Figure 11 and Figure 12, it can be seen that the plots are rotated clockwise and anti-clockwise for $\theta = 90°$ and $\theta = 0°$ respectively. The unsymmetrical contour plots also mean that the effect of the two differential polarisability ratios is no longer the same. According to Figure 12(a), the R value at $\theta = 0°$ is not sensitive to a change in the value of b when $b > -0.5$. However, the R is doubled by decreasing a from 0 to -0.5. The R value at $\theta = 90°$ is also doubled according to Figure 12(b).

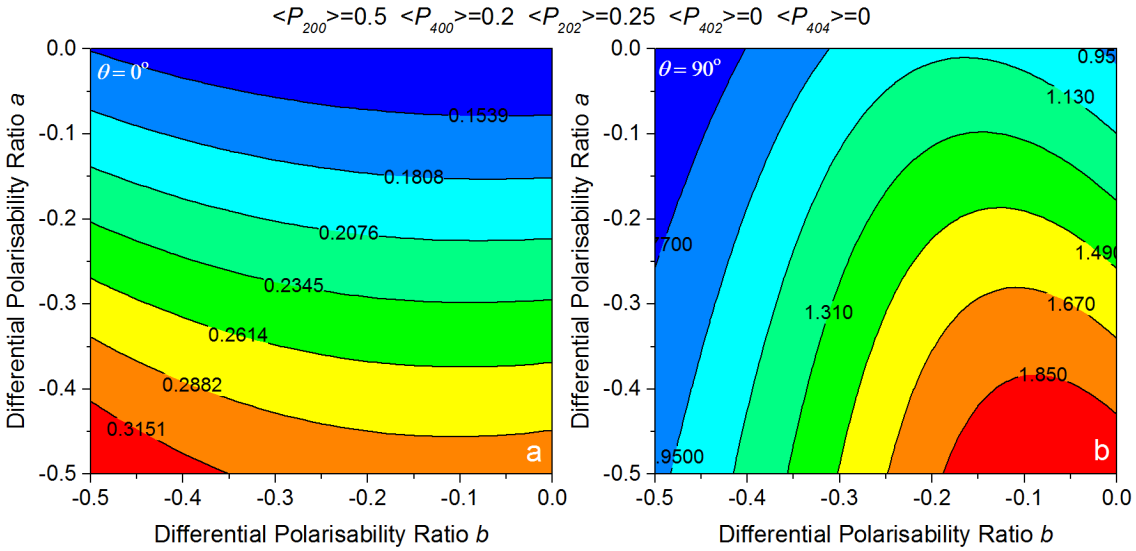

Figure 12. The contour plot of the depolarisation ratio R at: a) $\theta = 0°$ and b) $\theta = 90°$ with $\langle P_{200} \rangle = 0.5$, $\langle P_{200} \rangle = 0.2$, $\langle P_{202} \rangle = 0.25$, $\langle P_{402} \rangle = 0$ and $\langle P_{404} \rangle = 0$. The x axis and y axes are differential polarisability ratios b and a respectively.

In Figure 13, $\langle P_{402} \rangle$ is set to be 0.536 while the other molecular biaxial order parameters are set to zero. The contour plots are again asymmetrical, and qualitatively, the effect of $\langle P_{402} \rangle$ on the depolarisation ratio is similar to that of $\langle P_{202} \rangle$. However, the amounts of change in R is different; the range of R is almost 4 times the minimum value for the case of Figure 13 compared to only 2 or 3 times in Figure 12.

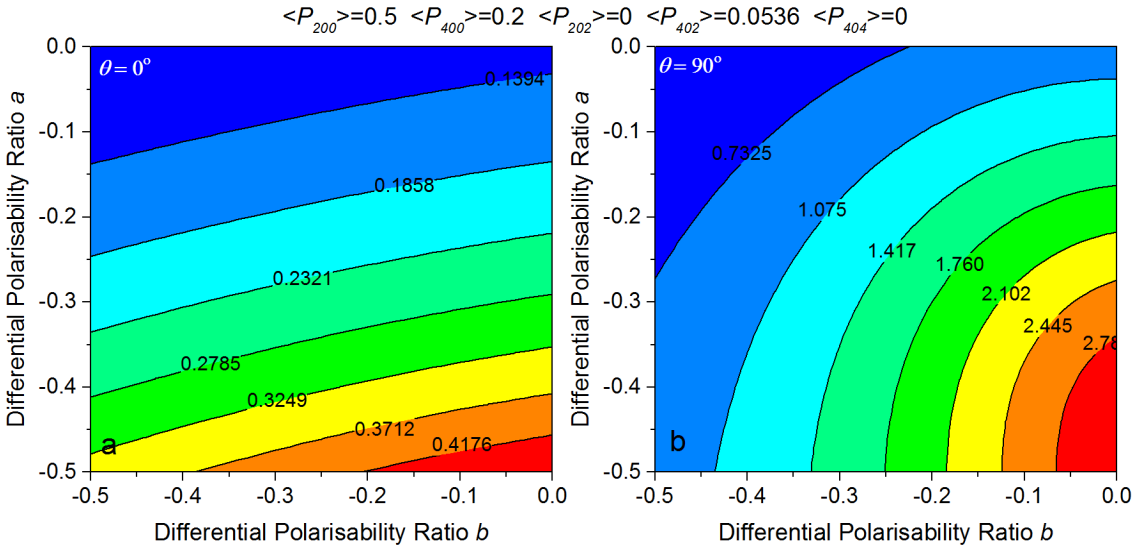

Figure 13. The contour plot of the depolarisation ratio R at: a) $\theta = 0°$ and b) $\theta = 90°$ with $\langle P_{200} \rangle = 0.5$, $\langle P_{200} \rangle = 0.2$, $\langle P_{202} \rangle = 0$, $\langle P_{402} \rangle = 0.536$ and $\langle P_{404} \rangle = 0$. The x axis and y axes are differential polarisability ratios b and a respectively.

Finally, the contour plots found after introducing $\langle P_{404} \rangle$ are shown in Figure 14. In these contour plots, $\langle P_{404} \rangle$ is set to be 0.625 while other molecular order parameters are still zero. Obviously the plots in Figure 14 are symmetric due to the $(a - b)^2$ term. The symmetrical contour plots indicate that the two differential polarisability ratios, a and b, have exactly the same effect on R. However, there is an important difference between Figure 14(a) and Figure 11(a), namely the curvature direction. This difference indicates a decrease in R for $\theta = 0°$ when $a \neq b$ due to the existence of $\langle P_{404} \rangle$. On the other hand, the R value at 90° for the same a and b values also decreases due to $\langle P_{404} \rangle$ (see Figure 14(b) and Figure 11(b)).

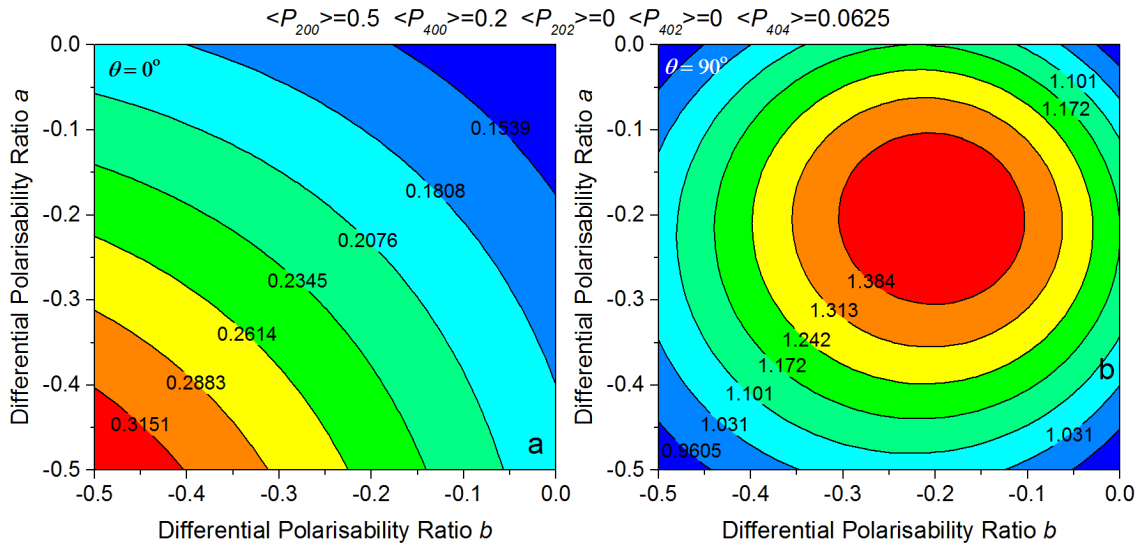

Figure 14. The contour plot of the depolarisation ratio R at: a) $\theta = 0°$ and b) $\theta = 90°$ with $\langle P_{200} \rangle = 0.5$, $\langle P_{200} \rangle = 0.2$, $\langle P_{202} \rangle = 0$, $\langle P_{402} \rangle = 0$ and $\langle P_{404} \rangle = 0.0625$. The x axis and y axis are the differential polarisability ratios b and a respectively.

Discussion of the non-cylindrical symmetric vibration model

It can be concluded that if there are two distinct differential polarisability ratios a and b, there is a strong effect on the depolarisation ratio value. Unfortunately, such a strong dependency of a and b would introduce a huge uncertainty to the fitting process if we were to try to include it. Moreover, the molecular biaxial order parameters introduced when $a \neq b$ cause a further strong degeneracy in the fitting process. Consequently, rather than attempting to fit the experimental data, Figure 15 shows two calculated depolarisation ratio graphs with strong similarities to the experimental data obtained from the cyano and phenyl stretching modes, Figure 3. To generate the calculated curves, we first fit the depolarisation ratio data from the phenyl stretching mode using Eqs.11 and 12 by setting a=b and all molecular biaxial order parameters to zero. Actually at this stage, it does not matter what the molecular biaxial order parameter values are as there is no effect on the intensity due to the $(a - b)$ term. Then we set the molecular biaxial order parameters to values based on LZNS

predications and finally obtained the fitting value of a and b using Eqs.11 and 12 with all order parameters fixed. The black line in Figure 15 is comparable to the phenyl stretching mode (a and b share the same value) while the red line is similar to the cyano stretching mode with two different differential polarisability ratios a and b.

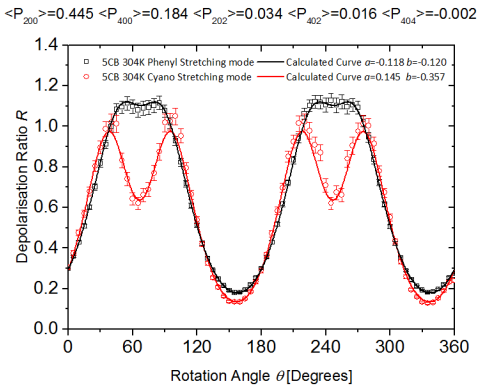

Figure 15. Two calculated depolarisation ratio graphs from eqs.11 and 12 with same set of order parameters: $\langle P_{200}\rangle = 0.445$, $\langle P_{400}\rangle = 0.184$, $\langle P_{202}\rangle = 0.034$, $\langle P_{402}\rangle = 0.016$ and $\langle P_{404}\rangle = -0.002$. Two different sets of polarisability ratios are used. The black line has a= -0.118 and b= -0.120 while the red line has a= 0.145 and b= -0.357

The result shown in Figure 15, suggests an explanation of why different order parameter values can be obtained from different vibrational modes. In this explanation, the phenyl stretching mode and the cyano stretching mode have different vibrational symmetries. For the phenyl stretching mode, the vibration is or close to cylindrically symmetric, satisfying the assumption in Jones' method. There is no difference or the difference is tiny between the two differential polarisability ratios and thus the molecular biaxial order parameters do not have strong effect on the depolarisation graph. As a consequence, Jones's method works well for this vibrational mode. In fact, according to Ref.4, $\langle P_{400}\rangle$ obtained from the phenyl stretching mode using Jones' method are also somewhat higher than the value obtained from X-ray data when compared with theoretical predictions of Maier Saupe and HJL theory. This may also indicates some level of non-cylindrical symmetry even in

phenyl stretching mode, agreeing with Jen and Miyano's statements [17, 25]. On the contrary, if the vibration for the cyano stretching mode has non-cylindrical symmetry, breaking the assumption, the difference between the two differential polarisability ratios must be included and the molecular biaxial order parameters generate a strong modification on the depolarisation graph. In such a case, Jones' method cannot provide a robust order parameters.

Conclusions

In this paper, we have considered two approaches to try to understand the origin of the discrepancy in order parameters obtained from different vibrational modes in Raman analysis. In the first approach, we considered a non-axial model by introducing a vibrational tilt β_0 into the analysis. The second approach considered a non-cylindrical vibration symmetry model by introducing two different differential polarisability parameters into the analysis. These two approaches both included molecular biaxial order parameters. A systematically discussion of each case has allowed a deep insight into the problem. It is clear that the phenyl stretching mode in these liquid crystal molecules largely satisfies the assumptions of Jones' method. However, molecular biaxial order parameters alongside the different differential polarisability parameters and vibrational tilt can also play an important role in the analysis of the cyano stretching mode, and very different order parameter values, especially for $\langle P_{400} \rangle$, are obtained if these considerations are neglected, as is the norm.

Although initially it might seem that either modification could explain the discrepancies shown in Figure 3, it is clear that there are a number of problems with the non-axial model. Firstly, fitting with non-axial model is not as robust as it would be necessary for routine use, due to the uncertainty introduced by the large number of fitting parameters. Further, one of the molecular biaxial order parameters always tended towards its theoretical limit and perhaps most importantly,

the tilt needed to be large for any significant effect, neither of which is physically realistic. Indeed the molecular modelling suggested negligible vibrational tilt. We therefore conclude that for this system, whether or not the vibrational satisfies the conditions of cylindrical symmetry is the correct physical explanation of the discrepancy seen experimentally in analysis of the Raman depolarisation ratio to determine the order parameters. Unfortunately, it is again not possible to carry out robust fitting to the experimental data with non-cylindrical symmetric model due to the strong degeneracy for different differential polarisability ratio parameters. We conclude that although we have offered a useful insight into the influence of various possible outcomes if the assumptions of Jones's analysis for Raman scattering aren't satisfied, it is not possible to deduce further parameters from the limited information available in the depolarisation ratio plots. Consequently, although we can understand why the analysis of different Raman active modes does not result in the same order parameter, hence solving a long-standing problem, we cannot offer a robust approach to allow any vibrational mode to be utilised and conclude that use of the 1606 cm^{-1} mode will result in the most physically realistic order parameters in most nematic systems.

Acknowledgement

We would thanks Dr. J.C.Li for the use of Material Studio program and technique support in the University of Manchester. We would also thanks A. E. Hassett and J. T. Barrett, students at the University of Manchester, for their help on data collection. The measurements were undertaken at the University of Manchester with this paper written after both Z. Zhang and H. F. Gleeson moved to their current address.

References

1. Luckhurst GR, Yeates RN. Orientational order of a spin probe dissolved in nematic liquid-crystals - electron resonance investigation. Journal of the Chemical Society-Faraday Transactions II. 1976;72:996-1009.
2. Matsuura K, Kotake Y, Kuwata K. Orientation of small molecules in a nematic liquid-crystal as studied by electron-spin-resonance. Molecular Crystals and Liquid Crystals. 1986;140:327-333.
3. Sanchez-Castillo A, Osipov MA, Giesselmann F. Orientational order parameters in liquid crystals: A comparative study of x-ray diffraction and polarized Raman spectroscopy results. Physical Review E. 2010;81:021707.
4. Leadbetter AJ, Norris EK. Distribution functions in 3 liquid-crystals from x-ray-diffraction measurements. Molecular Physics. 1979;38:669-686.
5. Deutsch M. Orientational order determination in liquid-crystals by x-ray-diffraction. Physical Review A. 1991;44:8264-8270.
6. Somashekar R, Somashekarappa H, Divya AP, et al. Orientational distribution function in nematic liquid crystals by x-rays: Fourier method. Pramana-Journal of Physics. 1999 ;52:67-74.
7. Giesselmann F, Germer R, Saipa A. Orientational order in smectic liquid-crystalline phases of amphiphilic diols. Journal of Chemical Physics. 2005;123:034906.
8. Davidson P. X-ray diffraction by liquid crystalline side-chain polymers. Progress in Polymer Science. 1996;21:893-950.
9. Gleeson HF, Southern CD, Brimicombe PD, et al. Optical measurements of orientational order in uniaxial and biaxial nematic liquid crystals. Liquid Crystals. 2010;37:949-959.
10. Richardson RM, Allman JM, McIntyre GJ. Neutron-scattering from mixtures of isotopically labeled molecules a new method for determining the orientational distribution function in liquid-crystals. Liquid Crystals. 1990;7:701-719.
11. Hamley IW, Garnett S, Luckhurst GR, et al. Orientational ordering in the nematic phase of a thermotropic liquid crystal: A small angle neutron scattering study. Journal of Chemical Physics. 1996;104:10046-10054.
12. Ossowska-Chrusciel MD, Korlacki R, Kocot A, et al. Infrared study of orientational order parameters of a ferroelectric liquid crystal. Physical Review E. 2004;70:041705.

13. Hild E, Kocot A, Vij JK, et al. Infrared spectroscopic study of a phenyl benzoate side-group methacrylate main-chain polymeric liquid-crystal. Liquid Crystals. 1994;16:783-803.
14. Kim KH, Ishikawa K, Takezoe H, et al. Orientation of alkyl chains and hindered rotation of carbonyl groups in the smectic-c-asterisk phase of antiferroelectric liquid-crystals studied by polarized fourier-transform infrared-spectroscopy. Physical Review E. 1995;51:2166-2175.
15. Sanchez-Castillo A, Osipov MA, Jagiella S, et al. Orientational order parameters of a de Vries-type ferroelectric liquid crystal obtained by polarized Raman spectroscopy and x-ray diffraction. Physical Review E. 2012;85:061703.
16. Jen S, Clark NA, Pershan PS, et al. Raman-scattering from a nematic liquid-crystal - orientational statistics. Physical review letters. 1973;31:1552-1556.
17. Jen S, Clark NA, Pershan PS, et al. Polarized raman-scattering studies of orientational order in uniaxial liquid-crystalline phases. Journal of Chemical Physics. 1977;66:4635-4661.
18. Jones WJ, Thomas DK, Thomas DW, et al. On the determination of order parameters for homogeneous and twisted nematic liquid crystals from Raman spectroscopy. Journal of Molecular Structure. 2004;708:145-163.
19. Jones WJ, Thomas DK, Thomas DW, et al. Raman scattering studies of homogeneous and twisted-nematic liquid crystal cells and the determination of $< P_2 >$ and $< P_4 >$ order parameters. Journal of Molecular Structure. 2002;614:75-85.
20. Zhang ZP, Panov VP, Nagaraj M, et al. Raman scattering studies of order parameters in liquid crystalline dimers exhibiting the nematic and twist-bend nematic phases. Journal of Materials Chemistry C. 2015;3:10007-10016.
21. Southern CD, Gleeson HF. Using the full Raman depolarisation in the determination of the order parameters in liquid crystal systems. European Physical Journal E. 2007;24:119-127.
22. Hayashi N, Kato T, Fukuda A, et al. Evidence for de Vries structure in a smectic-A liquid crystal observed by polarized Raman scattering. Physical Review E. 2005;71:041705
23. Maier W, Saupe A. Eine einfache molekulare theorie des nematischen kristallinflussigen zustandes. Zeitschrift fur naturforschung part a-astrophysik physik und physikalische chemie. 1958;13:564-566.
24. Humphrie.Rl, James PG, Luckhurs.GR. Molecular field treatment of nematic liquid-crystals. Journal of the Chemical Society-Faraday Transactions II. 1972;68:1031-1044.

25. Miyano K. Raman depolarization ratios and order parameters of a nematic liquid-crystal. Journal of Chemical Physics. 1978;69:4807-4813.
26. Vangurp M. The use of rotation matrices in the mathematical-description of molecular orientations in polymers. Colloid and polymer science. 1995;273:607-625.
27. Jarvis DA, Hutchinson IJ, Bower DI, et al. Characterization of biaxial orientation in poly(ethylene-terephthalate) by means of refractive-index measurements and raman and infrared spectroscopies. Polymer. 1980;21:41-54.
28. Luckhurst GR, Zannoni C, Nordio PL, et al. Molecular field-theory for uniaxial nematic liquid-crystals formed by non-cylindrically symmetric molecules. Molecular Physics. 1975;30:1345-1358.